Journal of Ultrafine Grained and Nanostructured Materials
https://jufgnsm.ut.ac.ir
Vol. 59, No.1, June 2026, pp. 150-160
Print ISSN: 2423-6845 Online ISSN: 2423-6837
DOI: 10.22059/jufgnsm.2026.01.11

Crystallization of the $Fe_{82.9}Si_{4.2}B_{12.3}C_{0.6}$ Amorphous Alloy Under a 2 Tesla Static Magnetic Field

Mehdi Sadegh-Ahmadi[1], Mohammadali Ebadi[1], Hamid Reza Madaah-Hosseini[1,2]*

[1] Department of Materials Science and Engineering, Sharif University of Technology, Azadi Avenue, Tehran, Iran, P.O. Box: 1458889694.
[2] Center for Bioscience and Biotechnology, Institute for Convergence Science and Technology, Sharif University of Technology, Tehran, Iran, P.O. Box: 1458889694.

Recieved: 19 May 2026; Accepted: 23 June 2026

*Corresponding author, E-mail: Madaah@Sharif.edu

ABSTRACT

This study investigates the crystallization behavior of a 20 µm thick $Fe_{82.9}Si_{4.2}B_{12.3}C_{0.6}$ amorphous ribbon under a 2 T magnetic field applied parallel to the sample surface. This phase transformation was characterized using X-ray Diffraction (XRD) and Differential Scanning Calorimetry (DSC) techniques. The results demonstrate that the magnetic field inhibits the formation of the bcc α-Fe(Si) phase at relatively low temperatures (480 and 490 °C), while it slightly reduces the crystallization rate at an elevated temperature of 520 °C. The underlying phase transformation mechanisms remain unchanged in the presence of the magnetic field. Application of the magnetic field at 520 °C for 15 min results in significant refinement of the α-Fe grains, reducing their average size from 53 nm to 48 nm and decreasing the crystallinity from 45% to 42%. These findings indicate that the magnetic field influences α-Fe nucleation through two competing effects: i) an excess magnetic driving force that promotes nucleation, and ii) a reduction in growth rate arising from decreased atomic diffusivity. The balance between these two factors governs the overall kinetics of crystallization. In contrast to previous studies, the dominant effect observed in the present study under a 2 T magnetic field is the reduced diffusivity of the rate-controlling element, silicon.

Keywords: *FeSiB-based Amorphous Alloy, Magnetic Field Annealing, Crystallization Kinetics, Non-Isothermal DSC Analysis, XRD Measurement.*

1. Introduction

Strong magnetic fields significantly influence the kinetics and thermodynamics of phase transformations in steel alloys [1, 2]. By applying an external magnetic field, the nuclei of ferromagnetic phases such as α-Fe become readily magnetized, leading them to a lower energy state. Consequently, the formation of such phases in steel alloys can be facilitated in the presence of external magnetic fields, provided that the heat treatment is performed below the Curie temperature of the newly formed phase, thereby preserving its ferromagnetic properties. Joo et al. reported that the temperature of the α/γ phase transformation in plain steel rose by 10 °C when subjected to a magnetic field of 20 Tesla [3]. This indicates that the magnetic field encourages the formation of ferromagnetic α-Fe within the paramagnetic γ-Fe matrix. Similarly, the overall kinetics of phase transformation have been reported to increase markedly in bainitic and maraging steels upon the application of strong magnetic fields [4, 5]. These results highlight how the magnetic field enhances the driving force for forming ferromagnetic phases within a paramagnetic parent phase.

Nanocrystalline alloys based on the FeSiB system represent a novel family of soft magnetic materials. These alloys are characterized by the formation of nano-sized α-Fe or ordered FeSi phases embedded within an amorphous parent phase via the process of nanocrystallization [6, 7]. This process is often conducted at temperatures exceeding the Curie temperature of the initial amorphous alloy, resulting in the precipitation of a ferromagnetic crystalline phase within a paramagnetic amorphous matrix [8, 9]. Numerous researchers have investigated the effects of strong magnetic fields on the kinetics of nanocrystallization, an area essential for understanding the final microstructure and magnetic properties of FeSiB-based nanocrystalline alloys [10-14], particularly the commercially available FineMet® alloy [15, 16].

Previous studies have shown that the kinetics of α-Fe crystallization were substantially enhanced when a strong magnetic field of 6 T was applied to $Fe_{78}Si_9B_{13}$ and 15 T to $Fe_{83.5}Si_{4.2}B_{12.5}$ amorphous alloys [12, 14]. Although only minimal changes in the nanocrystallization kinetics were observed at relatively lower magnetic fields (2 T for $Fe_{78}Si_9B_{13}$ and 1 T for $Fe_{80}Si_9B_{11}$), a notable refinement of the α-Fe phase was achieved in the latter study [12, 13]. The volume fraction of the crystalline phase in FineMet® alloy was reported to increase after annealing under a 2 T magnetic field, which was linked to rapid nucleation rather than accelerated growth [15]. In summary, it is generally believed that external magnetic fields can influence the nanocrystallization process by a) reducing the grain size through an increased nucleation rate and b) enhancing the overall kinetics, thereby increasing the volume fraction of the crystalline phase.

However, conflicting results have been reported in the literature. Onodera et al. found that applying a 10 T magnetic field promoted α-Fe phase formation in the $Fe_{83.5}Si_{4.2}B_{12.5}$ amorphous alloy [14], yet the same field was reported to suppress this phase transformation in $Fe_{79}Si_{12}B_9$ [9]. Such discrepancies, along with broader variability in the reported effects of magnetic fields on nanocrystallization, highlight the need for further systematic investigation into how external magnetic fields influence this thermally activated phase transformation. This study examines the effect of a moderately intense magnetic field of approximately 2 T, a magnitude that is economically viable for industrial applications, on the crystallization kinetics of the α-Fe phase in the $Fe_{82.9}Si_{4.2}B_{12.3}C_{0.6}$ (in atomic percent) amorphous alloy. This alloy was selected because it exhibited slow nucleation and rapid growth of the α-Fe phase, creating a challenging environment for effective nanocrystallization. This work aims to determine whether a moderate magnetic field can enhance the kinetics of nanocrystallization in such alloys.

2. Materials and Methods

A commercially available amorphous ribbon with the composition of $Fe_{82.9}Si_{4.2}B_{12.3}C_{0.6}$ (at. %) was selected for this research because it lacks any alloying elements that affect nucleation or growth of the α-Fe phase during crystallization. Therefore, it could be an adequate raw material for investigating the impact of an external magnetic field on the crystallization rate. The material was supplied as a 1.5 m long ribbon with a width of 18 cm and a thickness of 20 μm. Its chemical composition was verified using Inductively Coupled Plasma Optical Emission Spectroscopy (ICP-OES) and Non-Dispersive Infrared (NDIR) analysis. The chemical composition was consistent with the specifications of the alloy described in patent No. US20100175793A1.

All crystallization experiments were carried out in a quartz tube connected to a heating system that provided a continuous flow of hot argon gas, ensuring a stable temperature across the sample surface, with a variation measured to be as large as 3 °C. The tube was positioned between the poles of an air-cooled copper coil electromagnet capable of generating a magnetic field of up to 2 Tesla. The magnetic field was found to be uniform in the space between the poles, with field lines oriented parallel to the sample surface. For this purpose, 5 mm × 20 mm samples were cut from the as-received ribbons. The samples were subjected to heat treatment at various temperatures and durations of interest, both with and without the application of an external magnetic field. After heat treatment, the samples were air-cooled to room temperature.

The microstructure of the investigated samples was analyzed using a table-top X-ray diffraction (XRD) instrument with Cu-K_α radiation, both before and after crystallization experiments, to characterize the extent of microstructural changes. For this purpose, the samples were bonded to a single-crystal silicon substrate with a thin adhesive layer, which helped minimize unwanted X-ray scattering from the substrate and thereby enhanced the signal-to-noise ratio of the XRD spectra. The collected spectra were processed using Origin software for background removal. The refined data were then used to generate diffraction patterns or to perform Scherrer and Williamson-Hall analyses to determine key microstructural parameters such as grain size, lattice parameters, lattice strain, and the volume fraction (crystallinity) of the α-Fe phase within the surrounding amorphous matrix.

The Differential Scanning Calorimetry (DSC) technique was employed to measure the heat of crystallization for both the α-Fe phase and the

boride phases. In this study, samples with different heat treatment histories were analyzed using DSC. For this purpose, approximately 100 mg samples were prepared and placed in aluminum pans. The pans and their aluminum lids were tightly forged to enhance heat transfer during the DSC measurements. Multiple pieces, each no larger than 4 mm, were cut from the samples to ensure sufficient weight for reliable data collection. Furthermore, all measured heats of phase transformations in this study were normalized to the weight of the analyzed samples, enabling a quantitative analysis of the activation energy associated with the formation of the crystalline phases using the Flynn-Wall-Ozawa (FWO) formulation. Moreover, the local Avrami exponent for the α-Fe phase crystallization was calculated using the Matusita–Sakka method.

3. Results

3.1. XRD Analysis

Figure 1 presents the XRD patterns of the $Fe_{82.9}Si_{4.2}B_{12.3}C_{0.6}$ (at. %) alloy in its initial state (As-Received) and after heat treatment at temperatures of 480, 490, 520, and 540 °C under a magnetic field of 2 T (Field-Annealed) and without the magnetic field (Normal-Annealed). The absence of distinct diffraction peaks in the as-received sample indicates that the initial alloy possesses an amorphous microstructure lacking long-range atomic ordering. All samples subjected to heat treatment without the application of a magnetic field exhibited a diffraction at 44.85°, which corresponds to the (110) planes of the bcc α-Fe phase. The lattice parameter of the α-Fe phase was determined to be 2.859 Å in the sample heat-treated at 490 °C for 10 min, which is slightly smaller than that of pure α-Fe (2.866 Å). This difference can be attributed to the substitution of Si atoms within the lattice sites of α-Fe, resulting in a decrease in the average lattice parameter due to the smaller atomic size of Si compared to Fe. The formation of the bcc α-Fe(Si) phase has been documented in NANOMET® alloys, while the crystallization of an ordered FeSi phase with a DO_3 crystal structure is well-recognized in FINEMET® alloys [17, 18]. Furthermore, the XRD pattern of the sample heat-treated at 540 °C for 5 min displayed weak peaks at 42.61°, 49.86°, and 56.40°, indicating the presence of the Fe_2B phase, which is known to form in FeSiB-based alloys at relatively high temperatures. Consequently, the annealing temperature in this study was limited to 520 °C to prevent the formation of boride phases, which act as hard magnetic phases [6, 7].

The 110 diffraction peak of the α-Fe phase was observed in all samples subjected to heat treatment in the absence of the magnetic field. This peak intensified with either higher temperatures or prolonged crystallization times, indicating that the volume fraction of the α-Fe phase (hereafter referred to as crystallinity) increases within the parent amorphous matrix. The crystallinity can be estimated by calculating the ratio of the area under

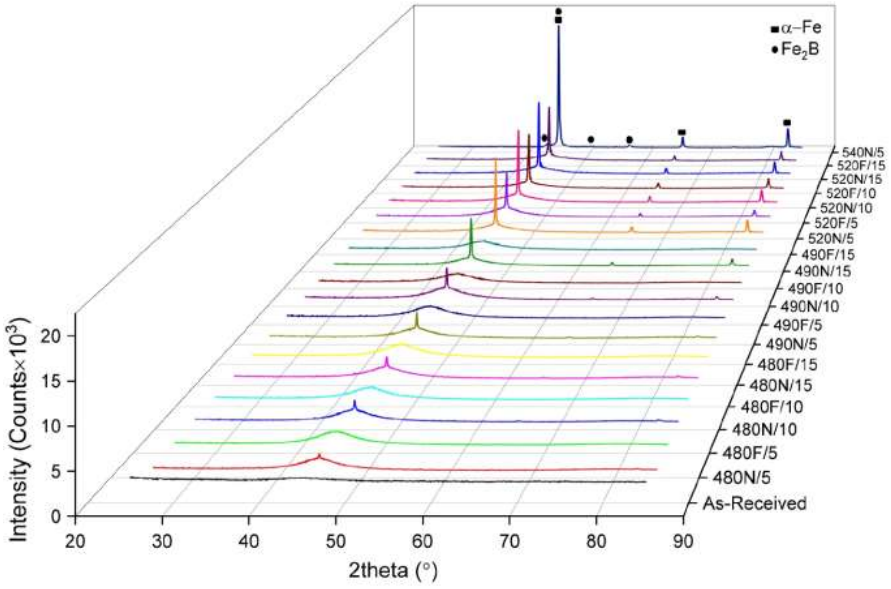

Fig. 1- The XRD patterns of the $Fe_{82.9}Si_{4.2}B_{12.3}C_{0.6}$ alloy before and after heat treatment under various conditions (N=Normal-Annealed, F=Field-Annealed, 480F/5= Field-Annealed at 480°C for 5 min). The external magnetic field significantly reduced the crystallization rate of the α-Fe phase.

diffraction peaks of the α-Fe phase to the total area, which also includes the broad background mainly arising from the amorphous phase. As crystallinity increases, additional but weaker diffraction peaks corresponding to the (200) and (211) planes of the α-Fe phase also emerge. Notably, the lattice parameter of the α-Fe phase was measured to decrease from 2.863 Å in the sample heat-treated at 480 °C for 5 min to 2.855 Å in the sample heat-treated at 540 °C for 5 min, indicating that the lattice parameter of the α-Fe phase declines as crystallization progresses at elevated temperatures. Figure 2 illustrates the evolution of the lattice parameter and crystallinity of the α-Fe phase as a function of temperature. Such behavior is attributed to the diffusion of Si atoms from the amorphous parent phase and their subsequent enrichment in the growing α-Fe phase. It suggests that Si serves as the rate-controlling element for the overall diffusion rate in this alloy. Although elements such as C and B may also influence the diffusion rate to some extent, their impact is considerably smaller due to their much smaller atomic radii.

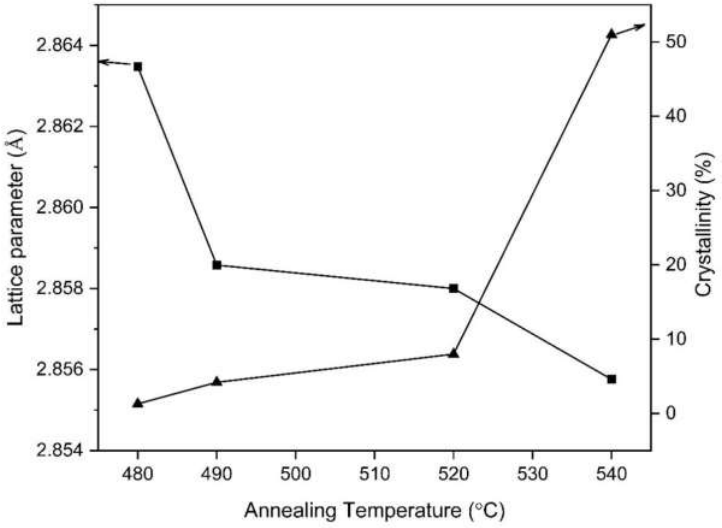

Fig. 2- Variation of the lattice parameter and volume fraction of the α-Fe phase as a function of annealing temperature, at 5 min annealing time. The reduction in lattice parameter is attributed to the enrichment of silicon atoms within the α-Fe grains as crystallization progresses. The uncertainty in lattice parameter measurements is below 0.002 Å.

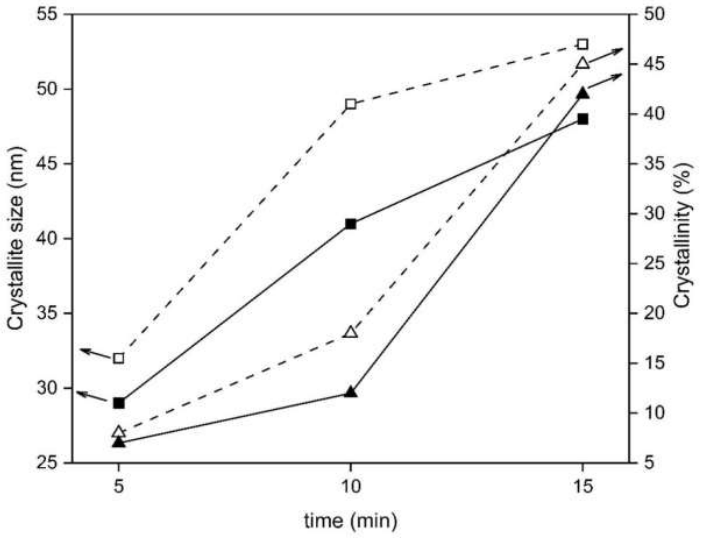

Fig. 3- Evolution of the average grain size and volume fraction of the α-Fe phase during prolonged crystallization at 520 °C, both with (solid lines) and without (dashed lines) a 2 T magnetic field. Pronounced α-Fe grain refinement is observed.

The XRD patterns presented in Figure 1 indicate that the application of an external magnetic field of 2 T inhibited the crystallization of the α-Fe phase in samples annealed at 480 °C and 490 °C, regardless of the annealing duration. Moreover, the kinetics of α-Fe phase formation were significantly suppressed in samples subjected to the magnetic field at 520 °C, with crystallinity decreasing from 45% to 42% after 15 min of annealing under the magnetic field (sample 520/F/15). Figure 3 illustrates the average grain size and volume fraction of the α-Fe phase as a function of annealing time at 520 °C, as determined by the Williamson-Hall method. Notably, the application of the magnetic field induced substantial grain refinement, reducing the average grain size from 53 nm in the sample crystallized without a magnetic field to 48 nm in the sample crystallized under a 2 T magnetic field, indicating a suppression of the growth rate of α-Fe nuclei. In addition to grain refinement, the observed reduction in the overall crystallization kinetics, i.e., the decreased crystallinity of α-Fe, contrasts with numerous previous studies that reported a positive effect of external magnetic fields on the nanocrystallization rate in FeSiB-based amorphous alloys. The observed reduction in crystal size appears to be more pronounced than the decrease in crystallinity, suggesting that the reduced growth rate was partially compensated by an increased nucleation rate.

3.2. DSC Analysis

The XRD results presented in Figure 1 revealed that the application of a 2 T magnetic field suppressed the crystallization of the α-Fe phase in the $Fe_{82.9}Si_{4.2}B_{12.3}C_{0.6}$ amorphous alloy. To validate these findings, an experiment employing a two-step heat treatment protocol was designed, as illustrated in Figure 4. Multiple 4*4 mm2 samples were prepared from the as-received amorphous ribbon and divided into three groups, each weighing no less than 100 mg. The first group remained in the initial amorphous state. The second group was crystallized at 490 °C for 5 minutes under a 2 T magnetic field, followed by air-cooling to room temperature. The third group underwent the same procedure but in the absence of the magnetic field. Samples in each group were combined for subsequent non-isothermal DSC analysis, ensuring that any potential chemical heterogeneity within the master batch and possible instrumental errors during the crystallization step, such as fluctuations in magnetic field strength or variations in sample temperature inside the quartz tube, could be mitigated in the final average result.

DSC measurements were performed on three groups of samples at three different heating rates (5, 10, and 20 K/min), following the protocol outlined in Figure 4. The resulting DSC curves are presented in Figure 5, where the exothermic peaks correspond to the formation of crystalline phases. As expected, these peaks shift to higher temperatures with

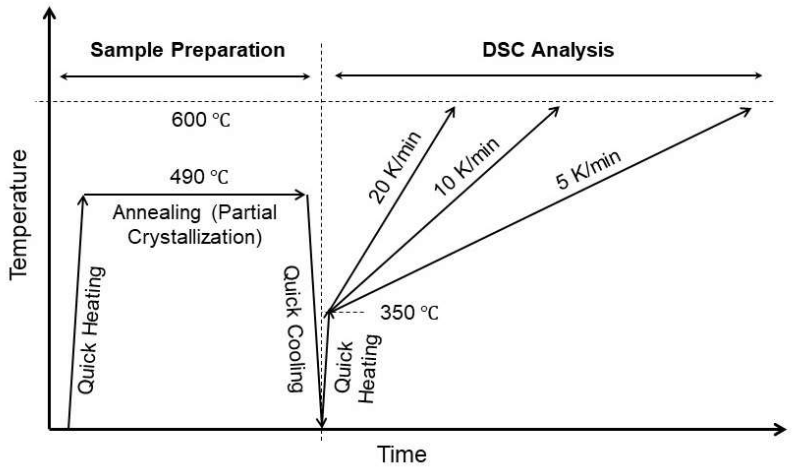

Fig. 4- Experimental protocol for a two-step crystallization of the as-received ribbon for quantitative DSC analysis. In the first step, samples were partially crystallized at 490 °C for 5 min, both in the presence and absence of an external magnetic field of 2 T. In the second step, as-received amorphous samples and partially crystallized samples were analyzed using the non-isothermal DSC method.

increasing heating rate. The first peak is attributed to the crystallization of the α-Fe phase, and the subsequent peak is associated with the formation of boride phases within the remaining B-rich amorphous matrix surrounding the α-Fe phase. The DSC results indicate that the formation of boride phases begins only after the crystallization of α-Fe is complete. In this study, the crystallization onset temperature (T_x) is defined as the temperature at which a given phase transformation reaches 1% progress. Notably, the measured T_x (T_{x2}-T_{x1}), which reflects the separation between the formation of these two crystalline phases, is smaller than that reported for NANOMET® and FINEMET® alloys [17, 18].

The heat of a given phase transformation can be quantified by integrating the area under the corresponding peak in the DSC curves. A larger peak corresponds to a greater volume fraction of the newly formed phase. As shown in Figure 5, the heat of α-Fe phase formation in the normal-annealed samples is significantly lower than that measured for the as-received amorphous alloy, indicating that a smaller amount of the α-Fe phase crystallized in the normal-annealed samples during the subsequent DSC step. This finding is consistent with the XRD results presented in Figure 1, indicating partial crystallization of the α-Fe phase at 490 °C during the first step of the experiment, thereby reducing the amount of α-Fe formed during the subsequent DSC measurement (see protocol in Figure 2).

Interestingly, the heat of α-Fe crystallization measured for the field-annealed samples during DSC analysis is relatively high, with values closely aligned to those of the as-received amorphous alloy. This suggests that the microstructure of the field-annealed samples closely resembles that of the as-received amorphous alloy, resulting in a similar thermodynamic response during DSC measurements. This finding is in perfect agreement with the XRD results shown in Figure 1, where the 110 diffraction peak of α-Fe completely disappears in samples annealed at 490 °C under a 2 T magnetic field, confirming that the magnetic field markedly suppressed the crystallization of the α-Fe phase in the $Fe_{82.9}Si_{4.2}B_{12.3}C_{0.6}$ amorphous alloy.

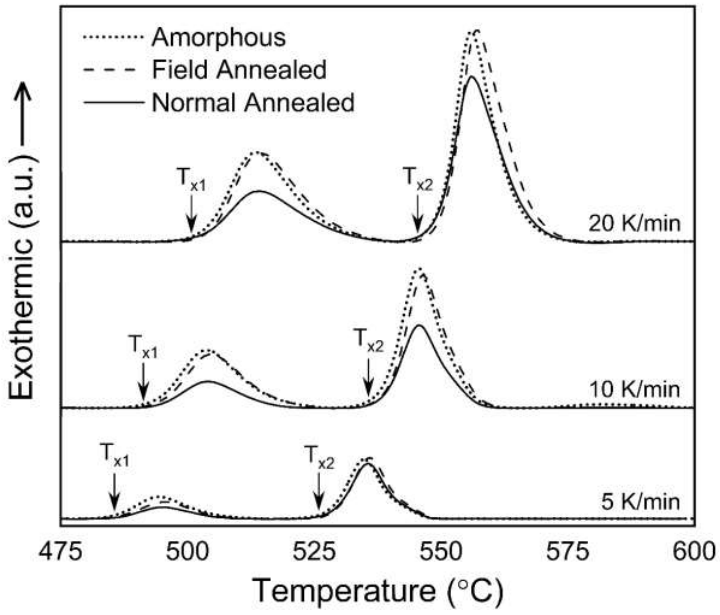

Fig. 5- DSC plots of the as-received amorphous alloy and the partially crystallized samples (see Fig. 2). Notably, the heat of crystallization for the field-annealed samples was found to be significantly higher than that of the normal-annealed samples, approaching that of the as-received alloy.

In this study, the local activation energy and Avrami exponent for α-Fe crystallization were determined in the three groups of samples from iso-conversional plots derived from DSC measurements. The progress of α-Fe crystallization at a given temperature was calculated as the ratio of the heat released up to that temperature to the total heat of crystallization. These values were then analyzed using the FWO method. Figure 6 presents the local activation energies for α-Fe phase formation within the amorphous matrix of the $Fe_{82.9}Si_{4.2}B_{12.3}C_{0.6}$ alloy. The local activation energy decreased from approximately 360 to 300 KJ/mol as crystallization progressed in the as-received sample. At the early stage of crystallization, the activation energy is associated with nucleation of the α-Fe phase, while the contribution of growth events becomes predominant at later stages. Accordingly, the activation energy for nucleation in this alloy was estimated to be approximately 360 KJ/mol, which is lower than that reported for the $Fe_{67}Nb_5B_{28}$ amorphous alloy (550-600 KJ/mol) [19]. The higher activation energy in the latter alloy is attributed to its relatively small driving force resulting from the low iron content, combined with slow diffusivity due to the presence of niobium. In contrast, the value obtained in the present study is higher than that measured for nucleation of the α-Fe phase in the $Fe_{83.3}Si_4B_8P_4Cu_{0.7}$ amorphous alloy (~ 270 KJ/mol), where nucleation occurs more readily in the presence of Cu [20].

The activation energy at the onset of α-Fe crystallization in the normal-annealed samples is higher than that of the as-received amorphous alloy, consistent with the higher T_{x1} measured in the normal-annealed samples (see Fig. 5). This finding indicates that the overall driving force for crystallization is reduced after the amorphous alloy undergoes partial crystallization (approximately 1.3%) during the first step of the protocol. In contrast, the activation energy for nucleation in the field-annealed samples is very close to that of the as-received samples, indicating that both groups of samples have similar microstructures and thermodynamic status before the DSC measurements. This is in perfect agreement with the XRD patterns (see Fig. 1), which reveal that crystallization was inhibited at 490 °C under a 2 T magnetic field. The local activation energy exhibits complex behavior at advanced stages of the phase transformation, indicating that a deeper understanding of the underlying mechanisms is required. As discussed below, this alloy undergoes weak and sluggish nucleation. When a 2 T external magnetic field is applied, a large number of α-Fe nuclei form during the first crystallization step. This promotes easier crystallization during the second step in the field-annealed and normal-annealed samples, as reflected by the rapid decrease in local activation energy once crystallization progresses beyond a certain extent.

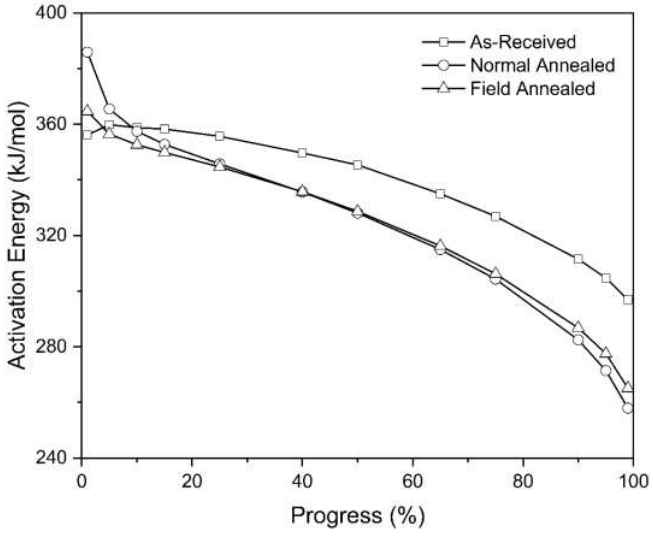

Fig. 6- Local activation energies for the crystallization of the α-Fe phase in the as-received amorphous alloy and the partially crystallized samples (see protocol in Fig. 4). Notably, the activation energy for nucleation in the field-annealed samples is significantly lower than that in the normal-annealed samples, with values closely matching those of the as-received alloy.

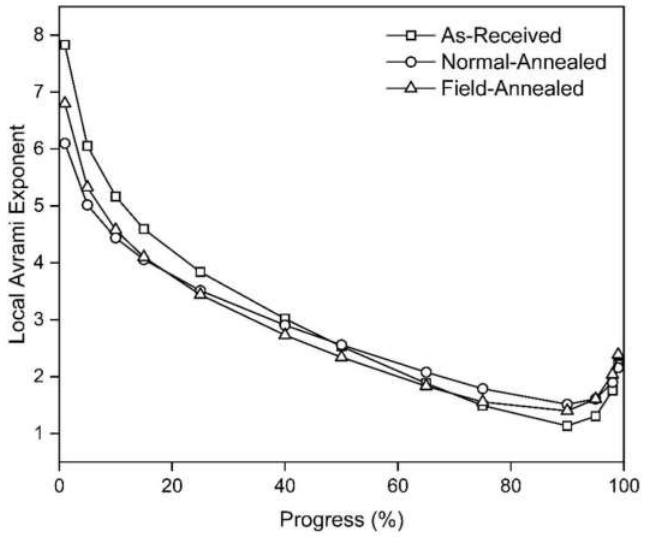

Fig. 7- Local Avrami exponent for crystallization of the α-Fe phase in as-received amorphous alloy and samples that were partially crystallized at 490 °C with and without the 2 T magnetic field.

Figure 7 presents the local Avrami exponent for α-Fe crystallization, determined from iso-conversional plots using the Matusita-Sakka formulation. The overall Avrami exponent reflects contributions from both nucleation and growth events. A very large Avrami exponent at the early stage (crystallized fraction less than 0.4) indicates that nucleation of α-Fe is the rate-controlling process, suggesting that the formation of a stable critical-sized nucleus is more challenging than subsequent growth. In contrast, the local Avrami exponent of approximately 1.5 at the later stages of crystallization indicates that the overall kinetics are predominantly governed by three-dimensional growth. During the intermediate stages, the kinetics become more complicated, as nucleation proceeds at a decreasing rate while previously formed α-Fe nuclei grow, accompanied by the depletion of Si atoms from the amorphous matrix and their enrichment in the α-Fe phase. Importantly, the phase transformation mechanism remained unaffected by prior crystallization, regardless of the application of a magnetic field. Therefore, the lower local activation energy observed in the partially crystallized samples (see Fig. 6) cannot be attributed to a change in the crystallization mechanism. Instead, this finding suggests that both groups of partially crystallized samples, irrespective of the crystallized fraction prior to the DSC measurements, contain a significant number of pre-existing α-Fe nuclei, thereby leading to a more substantial contribution from growth events in these samples.

4. Discussion

This study reveals that the crystallization of the α-Fe phase in the $Fe_{82.9}Si_{4.2}B_{12.3}C_{0.6}$ amorphous alloy proceeds via a nucleation and growth mechanism. Consequently, the overall activation energy of this phase transformation comprises the activation energies associated with nucleation events (Q_n) and the growth stage (Q_g). As illustrated in Figure 6, the overall activation energy decreases as the phase transformation progresses, while the growth of previously formed grains becomes the dominant phenomenon. This observation suggests that Q_g is lower than Q_n. Figure 7 shows that the Avrami exponent for crystallization of the α-Fe phase reaches a value of 1.5 after progress of approximately 0.8, indicating that α-Fe nuclei grow via a three-dimensional diffusion-controlled mechanism. Silicon is believed to govern the overall diffusion rate in this alloy, as its atomic size is smaller than that of elements such as boron and carbon [21, 22]. The activation energy for silicon diffusion in the $Fe_{82}B_{18}$ amorphous alloy has been reported to be 193 KJ/mol [23]. Considering the three-dimensional growth of α-Fe grains, Q_g can be estimated to be 1.5 times greater, i.e., around 290 KJ/mol, which is consistent with the results obtained in this study [24].

The nuclei of α-Fe form homogeneously within the amorphous matrix of $Fe_{82.9}Si_{4.2}B_{12.3}C_{0.6}$ alloy. Thus, the homogenous nucleation rate (N_{hom}) can be expressed as follows [24]:

$$N_{hom} = \omega C_0 \exp\left(-\frac{\Delta G_m}{kT}\right)\exp\left(-\frac{\Delta G^*}{kT}\right) \quad (1)$$

where C_0 represents the number of atoms per unit volume of the amorphous parent phase, ΔG^* is the activation energy for the formation of a nucleus of critical size, ω includes the vibrational frequency of atoms along with the cross-sectional area of the critical-sized nucleus, k is the Boltzmann constant, and T is temperature. Additionally, ΔG_m denotes the activation energy for atoms crossing the amorphous/crystalline interface. Due to the open atomic arrangement of the amorphous microstructure, ΔG_m is expected to depend on the diffusivity of silicon via a semi-interstitial mechanism [23]. By extracting the entropy terms, the activation energy of the nucleation event can be expressed as the sum of the enthalpy of migration (ΔH_m) and the enthalpy for the formation of critically sized nuclei (ΔH^*), given by:

$$Q_n = \Delta H_m + \Delta H^* \quad (2)$$

The ΔG^* term can be calculated by accounting for all driving forces involved in the crystallization of the α-Fe phase, under the assumption of constant surface energy (γ) with no orientation dependence [24]:

$$\Delta G^* = K\frac{\gamma^3}{(\Delta G_{ch} - \Delta G_s + \Delta G_{mag})} \quad (3)$$

where K is a factor that accounts for the morphology of the critically sized nucleus, ΔG_{ch} is the chemical driving force for this phase transformation, ΔG_s represents the elastic stain energy associated with the volumetric mismatch between the nucleus and the surrounding amorphous matrix, and ΔG_{mag} denotes an excess magnetic driving force that is often believed to facilitate the nucleation of the ferromagnetic α-Fe phase within the paramagnetic amorphous parent phase [13-15]. Consequently, an external magnetic field is expected to facilitate crystallization through a reduction in the ΔG^* term.

This study indicates that the α-Fe crystallization rate is likely influenced by the diffusivity of silicon atoms within the paramagnetic amorphous phase. Available reports on interdiffusion kinetics in the Fe-Si alloy system show a significant reduction in diffusivity under an external magnetic field of 0.8 T, while the activation energy for diffusion (ΔH_m) remained unchanged [25]. This was attributed to a decrease in the pre-exponential frequency factor of the diffusion coefficient, which is associated with the entropy term of diffusion (ΔS_m). Similar findings were observed in Al-Mg alloys subjected to a static magnetic field of 10 T, despite the paramagnetic nature of aluminum and magnesium, and regardless of the paramagnetic or diamagnetic characteristics of the intermediate phases [26, 27]. Additionally, the diffusivity of carbon in both the α (in ferromagnetic and paramagnetic states) and γ phases of iron has been reported to be influenced by external magnetic fields, with diffusivity decreasing as the magnetic field intensity increases [28]. These studies revealed that the activation energies for diffusion remained consistent under external magnetic fields, while the frequency factor changed due to the reduction of the entropy of diffusion [25, 27, 28].

The results in this study demonstrate that the overall rate of α-Fe crystallization in the $Fe_{82.9}Si_{4.2}B_{12.3}C_{0.6}$ amorphous alloy significantly decreases when subjected to an external magnetic field of 2 Tesla. It can be attributed to the diffusion-controlled growth of α-Fe nuclei, which is hindered by the 2 T magnetic field due to the decreased diffusivity of silicon (and, to a lesser extent, carbon and boron). On the other hand, the nucleation rate is influenced by two competing effects of the magnetic field: i) the magnetic field provides an access driving force that facilitates nucleation by lowering ΔG^*; and ii) conversely, it reduces diffusivity, making it more difficult for atoms to cross the amorphous/crystalline interface and attach to a critically sized nucleus to form stable nuclei. Thus, the overall impact of the magnetic field on the nucleation rate depends on which effect prevails. In this study, the effect of reduced diffusivity was found to be dominant, effectively inhibiting crystallization at relatively low temperatures (490 °C). However, at an elevated temperature of 520 °C, diffusivity was enhanced, allowing the formation of the α-Fe phase with refined grains under the magnetic field. Nonetheless, the volume fraction of the α-Fe phase reduced under the 2 T magnetic field even at 520 °C, suggesting that while nucleation may have occurred, its rate did not increase sufficiently to offset the decrease in the growth rate.

Considering only the density differences between the amorphous phase (7.19 g/cm^3) and the crystalline phase (~7.6 g/cm^3), and assuming no relaxation or morphological changes, the volumetric strain for α-Fe crystallization can be estimated to be as large as 5.5%, with tensile stresses applied to the crystalline phase. Notably, an elastic strain of about 8% has been reported to completely inhibit the formation of the equilibrium Zr_2Cu phase in the amorphous $Zr_{50}Cu_{40}Al_{10}$ alloy, leading to the formation of non-equilibrium transient phases [29]. This suggests that the influence of

elastic misfit energies must be considered in any quantitative modeling of α-Fe crystallization in FeSiB-based amorphous alloys, an area that has been largely neglected, to the author's knowledge.

5. Conclusions

In this study, contrary to many previous reports, a static uniform magnetic field of 2 T significantly reduced the overall kinetics of α-Fe crystallization in the $Fe_{82.9}Si_{4.2}B_{12.3}C_{0.6}$ amorphous alloy. Quantitative DSC analyses revealed that the overall phase transformation mechanism remained unchanged under the 2 T magnetic field; crystallization proceeds via homogeneous nucleation of the α-Fe phase, followed by three-dimensional growth controlled by the diffusion of atoms. The application of the magnetic field i) reduces silicon diffusivity, thereby lowering the growth rate and hindering nucleation by increasing the activation energy of migration (ΔG_m), and ii) promotes nucleation by decreasing its activation energy through an excess magnetic driving force. The observed reduction in the overall crystallization kinetics indicated that the decrease in diffusivity is the dominant effect in this study. Nonetheless, the contribution of the excess magnetic driving force becomes more pronounced during the nucleation stage, leading to grain refinement in samples crystallized under a 2 T magnetic field. Given that the alloy under investigation lacks elements that control the diffusion rate or facilitate nucleation, and considering its high iron content, the application of a magnetic field may offer new opportunities for tailoring the microstructure of similar alloys, particularly those governed by diffusion-controlled growth kinetics.

Acknowledgments

The authors kindly acknowledge M.Sc. Marziyeh Khaleqian's support in conducting the DSC experiments during this research.

References

1. Zhang Y, Esling C. The effect of a magnetic field on phase transformations in steels. In: Pereloma E, Edmonds DV, Editors. Phase Transformations in Steels: Fundamentals and Diffusion-Controlled Transformations, Woodhead Publishing; 2012, P. 555-580.
2. Liu XJ, Fang YM, Wang CP, Ma YQ. Effect of external magnetic field on thermodynamic properties and phase transitions in Fe-based alloys. Journal of Alloys and Compounds, 2008. 459(1): 169-173.
3. Joo HD, Kim SU, Koo YM, Shin NS, Choi JK. An effect of a strong magnetic field on the phase transformation in plain carbon steels. Metallurgical and Materials Transactions A, 2004. 35(6): 1663-1668.
4. Ohtsuka H. Effects of strong magnetic fields on bainitic transformation. Current Opinion in Solid State and Materials Science, 2004. 8(3): 279-284.
5. San Martin D, Van Dijk NH, Jiménez-Melero E, Kampert E, Zeitler U, Van Der Zwaag S. Real-time martensitic transformation kinetics in maraging steel under high magnetic fields. Materials Science and Engineering: A, 2010. 527(20): 5241-5245.
6. Herzer G. Modern soft magnets: Amorphous and nanocrystalline materials. Acta Materialia, 2013. 61(3): 718-734.
7. Gheiratmand T, Hosseini HRM. Finemet nanocrystalline soft magnetic alloy: Investigation of glass forming ability, crystallization mechanism, production techniques, magnetic softness and the effect of replacing the main constituents by other elements. Journal of Magnetism and Magnetic Materials, 2016. 408: 177-192.
8. Kaloshkin S, Churyukanova M, Zadorozhnyi V, Shchetinin I, Kumar Roy R. Curie temperature behaviour at relaxation and nanocrystallization of Finemet alloys. Journal of Alloys and Compounds, 2011. 509: 400-403.
9. Onodera R, Kimura S, Watanabe K, Yokoyama Y, Makino Y, Koyama K. Isothermal Crystallization of Iron-Based Amorphous Alloys in a High Magnetic Field. MATERIALS TRANSACTIONS, 2013. 54(7): 1232-1235.
10. Onodera R, Kimura S, Watanabe K, Yokoyama Y, Makino A, Koyama K. Crystallization kinetics of high iron concentration amorphous alloys under high magnetic fields. Journal of Alloys and Compounds, 2014. 604: 8-11.
11. Miglierini M, Procházka V, Rüffer R, Zbořil R. In situ crystallization of metallic glasses during magnetic field annealing. Acta Materialia, 2015. 91: 50-56.
12. Fujii H, Tsurekawa S, Matsuzaki T, Watanabe T. Evolution of a sharp {110} texture in microcrystalline Fe78Si9B13 during magnetic crystallization from the amorphous phase. Philosophical Magazine Letters, 2006. 86(2): 113-122.
13. Wang C, Wu Z, Feng X, Li Z, Gu Y, Zhang Y, et al. The effects of magnetic field annealing on the magnetic properties and microstructure of Fe80Si9B11 amorphous alloys. Intermetallics, 2020. 118: 106689.
14. Onodera R, Kimura S, Watanabe K, Yokoyama Y, Makino Y, Koyama Y. Nucleation control for fine nano crystallization of Fe-based amorphous alloy by high-magnetic-field annealing. Journal of Alloys and Compounds, 2015. 637: 213-218.
15. Fujii H, Yardley V, Matsuzaki T, Tsurekawa S. Nanocrystallization of Fe73.5Si13.5B9Nb3Cu1 soft-magnetic alloy from amorphous precursor in a magnetic field. Journal of Materials Science, 2008. 43(11): 3837-3847.
16. Fan X, Zhu F, Wang Q, Jiang M. Effect of Magnetic Field Annealing on Microstructure and Magnetic Properties of FeCuNbSiB Nanocrystalline Magnetic Core with High Inductance. Applied Microscopy, 2017. 47: 29-35.
17. McHenry M, Johnson F, Okumura H, Ohkubo T, Ramanan VRV, Laughlin DE. The kinetics of nanocrystallization and microstructural observations in FINEMET, NANOPERM and HITPERM nanocomposite magnetic materials. Scripta Materialia - SCRIPTA MATER, 2003. 48(7): 881-887.
18. Ayers JD, Harris VG, Sprague JA, Elam WT, Jones HN. On the formation of nanocrystals in the soft magnetic alloy Fe73.5Nb3Cu1Si13.5B9. Acta Materialia, 1998. 46(6): 1861-1874.
19. Zhao BG, Kong LH, Song TT, Zhai QJ, Gao YL. Phase precipitation and isothermal crystallization kinetics of FeZrB amorphous alloy. Advances in Manufacturing, 2013. 1(3): 251-257.
20. Miao X, Wang YG, Guo M. Structural, thermal and magnetic properties of Fe–Si–B–P–Cu melt-spun ribbons: Application of non-isothermal kinetics and the amorphous random anisotropy model. Journal of Alloys and Compounds, 2011. 509(6): 2789-2792.
21. Zhu J, Pradell T, Clavaguera N, Clavaguera-Mora MT. The Composition Effect on the Nanocrystallization of Finemet Amorphous Alloys. MRS Online Proceedings Library, 1996. 457(1): 285-290.
22. Pradell T, Crespo D, Clavaguera N, Clavaguera-Mora MT. Diffusion controlled grain growth in primary crystallization: Avrami exponents revisited. Journal of Physics:

Condensed Matter, 1999. 10 (7): 3833.
23. Luborsky FE, Diffusion of silicon into amorphous FexB100−x. Journal of Applied Physics, 1983. 54(10): 5732-5738.
24. Porter DA, Easterling KE, Sherif MY. Phase Transformations in Metals and Alloys. 3 ed. 2009: CRC Press.
25. Fan L, Zhong Y, Xu Y, Shen Z, Zheng T, Ren Z. Effect of static magnetic field on microstructure and interdiffusion behavior of Fe/Fe–Si alloy diffusion couple. Journal of Alloys and Compounds, 2015. 645: 369-375.
26. Nishimura K, Imai K, Matsuda K, Nunomura N. Magnetic property of Al-Mg alloys and intermetallic compounds. Journal of Alloys and Compounds, 2021. 877: p. 160226.
27. Li ZF,Dong J, Zeng XQ, Lu C, Ding WJ, Ren ZM. Influence of strong static magnetic field on intermediate phase growth in Mg–Al diffusion couple. Journal of Alloys and Compounds, 2007. 440(1): 132-136.
28. Fujii H, Tsurekawa S. Diffusion of carbon in iron under magnetic fields. Physical Review B, 2011. 83(5): 054412.
29. Zhang, S, Ichitsubo T, Yokoyama Y, Yamamoto T, Matsubara E, Inoue A. Crystallization Behavior and Structural Stability of Zr50Cu40Al10 Bulk Metallic Glass. Materials transactions, 2009. 50: 1340-1345.